Analytica Chimica Acta 1278 (2023) 341721

Contents lists available at ScienceDirect

Analytica Chimica Acta

journal homepage: www.elsevier.com/locate/aca

High-precision simultaneous measurement of ^{187}Os, ^{186}Os, and ^{184}Os using 10^{13} Ω amplifiers and CDDs on NTIMS

Guiqin Wang [a,b,*], Yuling Zeng [a,c], Liang Qi [d], Wengui Liu [e,**], Jifeng Xu [f]

[a] State Key Laboratory of Isotope Geochemistry, Guangzhou Institute of Geochemistry, Chinese Academy of Sciences, Guangzhou 510640, China
[b] CAS Center for Excellence in Comparative Planetology, Hefei 230026, China
[c] University of Chinese Academy of Science, Beijing 100049, China
[d] Institute of Geochemistry, Chinese Academy of Sciences, Guiyang 550002, China
[e] China University of Geosciences, Wuhan 430074, China
[f] China University of Geosciences, Beijing 100083, China

HIGHLIGHTS

- Combining Faraday cups and CDDs for Os analysis.
- Simultaneous measurement for all Os isotopes and O isotopes

GRAPHICAL ABSTRACT

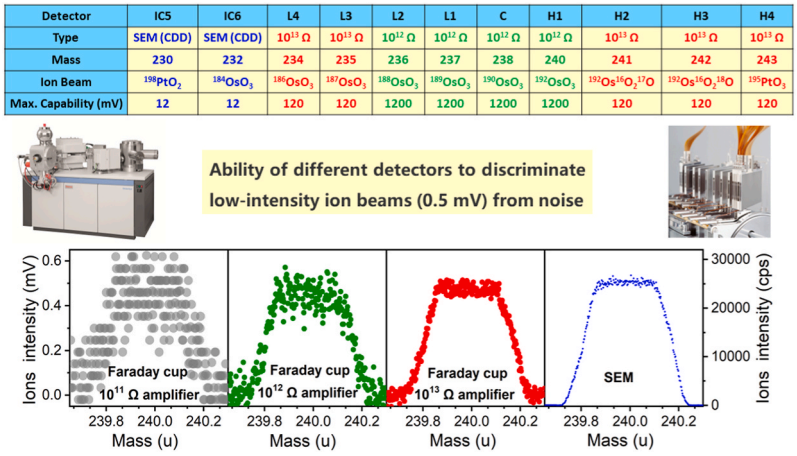

ARTICLE INFO

Handling Editor: Dr. L. Liang

Keywords:
Os isotopes
Small-size sample
NTIMS
10^{13} Ω amplifier

ABSTRACT

High-precision measurements of $^{184}Os/^{188}Os$, $^{186}Os/^{188}Os$, and $^{187}Os/^{188}Os$ ratios are significant in the fields of geochemistry and cosmochemistry. However, no high-precision measurement technique exists for simultaneously obtaining all three ratios using a static method for samples with an Os content of <1 ng or $^{186}OsO_3^-$ and $^{187}OsO_3$ ion-beam intensities of <150 mV. This greatly limits research on rare samples with small sample sizes or low Os contents, such as Lunar, Martian, or old Earth samples. This paper reports a static method, which could achieve the simultaneous measurement of 9 Faraday cups (FCs) with high-signal/noise ratio 10^{12} Ω amplifiers and 10^{13} Ω amplifiers and two compact discrete dynodes (CDDs). By analyzing two calibration solutions, a

* Corresponding author. State Key Laboratory of Isotope Geochemistry, Guangzhou Institute of Geochemistry, Chinese Academy of Sciences, Guangzhou 510640, China.
** Corresponding author.
E-mail addresses: guiqinwang@gig.ac.cn (G. Wang), liuwg@cug.edu.cn (W. Liu).

https://doi.org/10.1016/j.aca.2023.341721
Received 20 March 2023; Received in revised form 8 August 2023; Accepted 14 August 2023
Available online 14 August 2023

CDD
Static measurement

precision value of less than 3‰ (2RSD) could be achieved for $^{184}Os/^{188}Os$ ratios, even if the $^{184}OsO_3^-$ intensity was as low as 1000 cps. The precision values for the $^{186}Os/^{188}Os$ and $^{187}Os/^{188}Os$ ratios were similar and could be better than 0.066‰ (2RSD) when the intensities of $^{186}OsO_3^-$ and $^{187}OsO_3^-$ were greater than 30 mV, which can be obtained with conventional 10^{11} Ω amplifiers only at signals larger than 150 mV. Three geological reference materials were used in this study. The precision values of $^{184}Os/^{188}Os$, $^{186}Os/^{188}Os$, and $^{187}Os/^{188}Os$ ratios reached 2, 0.061, and 0.050‰ (2RSD), respectively, when the maximum Os amount was approximately 12 ng, and 87, 15, and 10‰ (2RSD), respectively, when the maximum Os amount was as low as approximately 66 pg. Additionally, our results show that changes in the volume of oxygen added during measurement can cause significant variations in the oxygen isotope composition. This static measurement method not only avoids the nonlinear signal change of the instrument during the analysis process but also realizes the accurate removal of the oxygen isobaric interference in the run, which could improve the precision of $^{184}Os/^{188}Os$, $^{186}Os/^{188}Os$, and $^{187}Os/^{188}Os$ ratios for small-size/low-signal samples.

1. Introduction

Accurate $^{184}Os/^{188}Os$, $^{186}Os/^{188}Os$, and $^{187}Os/^{188}Os$ ratios are vital for cosmochemical and geochemical research. Although several methods for regular sample sizes have successfully been applied in these fields, high-precision measurement of these Os isotopic ratios is still a challenge for samples with Os mass fractions of <1 ppb and/or sample weights of <2 g. To date, no high-precision analytical technique exists for simultaneously obtaining all three aforementioned ratios for samples with low Os contents and small sizes. Among the seven Os isotopes, ^{184}Os, ^{186}Os, and ^{187}Os are involved in the isotope systems ^{184}Os–^{180}W, ^{190}Pt–^{186}Os, and ^{187}Re-^{187}Os. The ^{187}Re-^{187}Os system is an irreplaceable chronological tool for the direct determination of the absolute ages of iron meteorites, metal deposits, petroleum systems, and sedimentary strata [1–6]. The ^{190}Pt–^{186}Os system is an important means of tracing core-mantle interactions in planetary systems and has received particular attention in the last two decades [7–13]. The ^{184}Os–^{180}W system could be used as a tracer and chronometer for important geological processes, such as core formation, silicate differentiation, or late accretion processes [14–17]. ^{184}Os is a p-process isotope [18,19] that provides a potential method for studying the distribution of p-process carriers in the early solar system. The precise determination of $^{184}Os/^{188}Os$, $^{186}Os/^{188}Os$, and $^{187}Os/^{188}Os$ ratios is a difficult task in these fields because their natural abundance is considerably low, especially for Lunar and Martian materials, not only because the available sample size is small but also because the abundances of Re, Pt, Os, and W are extremely low [20–24]. For all of the above reasons, research on Re–Os, Pt–Os, and Os–W isotope systems requires the development of an analytical technique for these samples. In previous studies, most measurements were conducted using Faraday cups (FCs) with conventional 10^{11} Ω amplifiers to analyze the ratios of $^{187}Os/^{188}Os$ and/or $^{186}Os/^{188}Os$ by negative thermal ionization mass spectrometry (NTIMS). However, the analysis of $^{184}Os/^{188}Os$ has rarely been reported [25–27] as the natural abundance of ^{184}Os is as low as 0.0002% [28] and accurate values cannot be obtained using FCs. In particular, the signals of $^{184}OsO_3^-$ cannot be identified by an FC with a 10^{11} Ω amplifier when they are lower than 0.1 mV which corresponding the ion beam signals of $^{186}OsO_3^-$ and $^{187}OsO_3^-$ are approximately 10 mV. In recent years, with the advent of 10^{12} Ω and 10^{13} Ω amplifiers, achieving high-precision determination for low-signal/small-size samples are theoretically possible. Several measurement methods have been reported using FCs with 10^{12} Ω or 10^{13} Ω amplifiers to collect Os isotopes by multi-collector-inductively coupled plasma mass spectrometry (MC-ICP-MS) or NTIMS [29–34]. Nevertheless, these methods only individually determine the ratios of $^{187}Os/^{188}Os$ and/or $^{186}Os/^{188}Os$ and not all three ratios of $^{186}Os/^{188}Os$, $^{187}Os/^{188}Os$, and $^{184}Os/^{188}Os$ simultaneously.

This paper presents a novel static measurement method to simultaneously determine 11 mass numbers, ranging from 230 to 243, using nine FCs connected to four 10^{12} Ω amplifiers and five 10^{13} Ω amplifiers and with the addition of two ion-counting detectors with a compact discrete dynode (CDD) by NTIMS. This static method can determine all seven Os isotopes in trioxides, $^{198}PtO_2$ and $^{195}PtO_3$ as monitors for Pt oxide interference, and $^{192}Os^{16}O_2^{17}O$ and $^{192}Os^{16}O_2^{18}O$ for calculating isotopic compositions of O. Moreover, the isobaric interferences of W and Re were measured before and after the analysis through a separate routine using a secondary electron multiplier (SEM; ion counter (IC) 1C). The new static measurement routine comprises a cup configuration combining 10^{13} Ω amplifiers, 10^{12} Ω amplifiers, and CDDs, making it suitable for the determination of small-size/low-Os content samples. Two single-element solution reference materials (SRMs) and three geological reference materials (GRMs) were analyzed using the proposed method. For all data in this study, the ion beam intensity of $^{185}ReO_3^-$ was less than 100 cps (~1.6 μV), and that of $^{183}WO_3^-$ was less than 20 cps (~0.4 μV). The $^{187}ReO_3/^{187}OsO_3$ and $^{186}WO_3/^{186}OsO_3$ ratios were always less than 0.2‰. This new method enables the acquisition of high-precision Os isotope ratios for small-size and/or low-content samples.

2. Experimental section

All the measurements were conducted using a Thermo Fisher Triton Plus thermal ionization mass spectrometer (TIMS) instrument at the State Key Laboratory of Isotope Geochemistry, Guangzhou Institute of Geochemistry, Chinese Academy of Science (GIG, CAS, Guangzhou, China).

2.1. Solution and geological reference materials

Two SRMs were used in this study: the Durham Romil Osmium Standard (DROsS, purchased from IAGeo Limited) and Leoben Osmium Standard (LOsT, provided by Dr. Meisel, T. C., Montanuniversität Leoben).

Additionally, three GRMs were chosen for their various lithologies and Os mass fractions: the United States Geological Survey (USGS) basalts BIR-1a and BHVO-2, and the Canadian Certified Reference Materials (CCRM; Ottawa, ON, Canada) altered peridotite WPR-1. These three GRMs are widely used for method validation and quality control in geochemistry and cosmochemistry. All GRM samples were purchased in the form of 200-mesh grain size. The Os mass fractions of the three GRMs ranged from approximately 76 pg g^{-1} to 13 ng g^{-1}. Each test portion of the rock sample weighed 0.87–0.91 g (Table 1). The GRMs

Table 1
Detailed information of geological reference materials in this study.

Name	Lithology	Mass fraction Os (pg g^{-1})	Weight (g)	Os amount (pg)
WPR-1	Peridotite	13,300	0.91	12,115
BIR-1a	Basalt	350	0.87	306
BHVO-2	Basalt	76	0.87	66

The Os mass fraction of WPR-1 was recommended by the supplier (CANMET-MMSL), and those of BIR-1a and BHVO-2 were obtained from a previous study conducted in our laboratory [34].

were dissolved in Carius tubes with inverse aqua regia (2.5 ml of concentrated HCl and 7.5 ml of concentrated HNO_3). The Carius tube opening was carefully sealed with high-temperature flame melting, and the tube was then heated in an oven at 230 °C for 48 h. Subsequently, Os was extracted using CCl_4, back-extracted into HBr, and finally refined using a microdistillation method [34,35]. The total procedural blanks were <0.4 pg and <2.1 pg for Os and Re, respectively.

2.2. Sample loading

Twenty and ten Pt filaments were loaded with approximately 20 ng of DROsS and LOsT, respectively. The purification Os of three rock samples (GRMs) was concentrated to approximately 1 μl at low temperature (80 °C) in HBr, and then separately loaded on a Pt filament.

High-purity Pt ribbons (99.995%, 0.025 mm × 1 mm) were purchased from the H. Cross Company (Moonachie, New Jersey, USA). The high-purity reagent $Ba(OH)_2{\cdot}8H_2O$ used for preparing the activators was purchased from Alfa Aesar China Co., Ltd. (Shanghai, China). The emitter $Ba(OH)_2$ was diluted to 3% $Ba(OH)_2{\cdot}8H_2O$ by weight in water. The high-purity Pt filaments were degassed at 3 A for 5 min in air before loading the samples. The Os isotopes were analyzed using a single-filament configuration.

2.3. Mass spectrometry

The TIMS is equipped with nine FCs with one 10^{11} Ω, four 10^{12} Ω, and five 10^{13} Ω amplifiers, and six ICs. Every cup could be flexibly connected to any amplifier to suit the measurements. The ICs include three classical SEMs with their deflection mechanisms (including IC 1C/B, IC2, and IC3A) and three SEMs with CDDs (including IC4, IC5, and IC6). The cryotrap, sample wheel, filament holder, extraction plate, and ion source used for the Os measurements in this study were systems dedicated to negative-ion Os isotope analyses. The instrument is equipped with an adjustable oxygen introduction device. To ensure a consistent frame of reference, we reported the ion beam intensities (V) relative to the 10^{11} Ω amplifiers. Therefore, we report a beam current of 3×10^{-14} A as an intensity of 3 mV independent of the amplifier type.

2.4. Measurement method

The cup configuration was set up for a static measurement routine involving nine FCs with 10^{12} Ω or 10^{13} Ω amplifiers and two CDDs (Table 2). Considering the different abundance of seven Os isotopes, four higher ion beams of $^{188}OsO_3^-$, $^{189}OsO_3^-$, $^{190}OsO_3^-$, and $^{192}Os^{16}O_3^-$ were collected by L2, L1, C, and H1 connected with four 10^{12} Ω amplifiers, respectively; $^{186}OsO_3^-$ and $^{187}OsO_3^-$ were collected by L4 and L3 connected with two 10^{13} Ω amplifiers, respectively; and $^{184}OsO_3^-$ was collected by a CDD of IC6. In addition to all seven Os isotopes, $^{195}PtO_3^-$ and $^{198}PtO_2^-$ were collected using H4 with a 10^{13} Ω amplifier and IC5 to monitor the platinum trioxide and dioxide interferences, respectively. Moreover, the oxygen isotopic composition was monitored by measuring $^{17}O^-$ and $^{18}O^-$-bearing molecular species for ^{192}Os at masses of 241 ($^{192}Os^{16}O_2^{17}O^-$) and 242 ($^{192}Os^{16}O_2^{18}O^-$) using H2 and H3 with 10^{13} Ω amplifiers. The largest beam size collected by FCs with 10^{12} Ω amplifiers should be lower than 1.2 V in the negative mode. Here, it corresponds to the ion beam of $^{192}Os^{16}O_3^-$ as no spike was used in this study. According to the natural abundance of Os isotopes, the ion beam sizes of $^{186}OsO_3^-$ and $^{187}OsO_3^-$ were less than 60 mV, and that of $^{184}OsO_3^-$ was lower than 0.6 mV. Owing to the limits on the current intensity involving both the 10^{13} and 10^{12} Ω amplifiers and CDDs, neither amplifier rotation nor multi-dynamic measurements were possible. To validate the accuracy and precision of $^{184}OsO_3^-$ by IC6, a subsequence cup configuration was set to use SEM (IC 1C) to analyze $^{184}OsO_3^-$ (mass of 232) for comparison. The subsequence cup configuration was only used to verify the accuracy of IC6 and the yield of the manual IC method but was not used when measuring samples.

In general, $^{185}ReO_3^-$ and $^{183}WO_3^-$ (or $^{182}WO_3^-$) were measured to monitor $^{187}ReO_3^-$, $^{184}WO_3^-$, and $^{186}WO_3^-$, which could cause isobaric interference in $^{187}OsO_3^-$, $^{184}OsO_3^-$, and $^{186}OsO_3^-$ measurements. As $^{185}ReO_3^-$ and $^{183}WO_3^-$ could not be aligned into the static main sequence, additional short interference runs were conducted before and after each data collection run. A peak-hopping method for SEM (IC 1C) runs was used to analyze $^{185}ReO_3^-$ and $^{183}WO_3^-$. This requires a clean instrument system, a chemical separation process with high Os recovery, and an extremely low background of Os and Re.

Additionally, as the instrument supplier does not provide an automatic calibration procedure for the yield of IC5 and IC6, we devised a new method for calibrating the yields of IC5 and IC6 by referring to the automatic procedure and the manual correction of the 10^{13} Ω amplifier's gain "cross calibration" procedure proposed by Wang et al. (2018) [36] (See Appendix A for details).

2.5. Measurement parameters

The Os isotope ratios were measured using a TIMS instrument in the negative ion mode. The baseline was conducted at the start of each day with a pre-wait time of 60 s, 1200 cycles, and an integration time per cycle of 1.05 s. Automatic gain calibration of the 10^{11}, 10^{12}, and 10^{13} Ω amplifiers was conducted once a week using a given virtual current of 0.12 V. The gains of the three types of amplifiers were calibrated by an automatic procedure, whose repeatability was similar and within 0.20–0.30‰ (2 RSD, t = 12 months). This long-term repeatability is consistent with those of <0.30‰ (2 RSD, t = 6 months), calibrated using the manual gain calibration method [36]. A software procedure (provided by the supplier) was used to correct the τ value for the different responses of signals measured simultaneously on the 10^{11}, 10^{12}, and 10^{13} Ω amplifiers. Each measurement comprised 200 ratios in 10 blocks over 20 cycles (Table 3). The integration time was 8 s for the main sequence (Seq. 1) and 4 s for the subsequence (Table 3: Seq. 2), wherein $^{184}OsO_3^-$ measured by the SEM (IC 1C) was to be compared with that by IC6. The idle time was set to 12 s to account for the slower response time of the 10^{13} Ω amplifiers for Seq. 1, and to 3 s for Seq. 2. During measurement, the oxygen pressure was maintained at $1.0–2.0 \times 10^{-7}$ mbar and adjusted by a needle valve. Each measurement lasted approximately 1.1 h excluding Seq. 2. To achieve the optimum peak overlap for the cup configuration, the focus and dispersion voltages were set to −8.0 and 33.0 V, respectively. The evaporation filament temperature for collecting the ion beam of SRMs ranged from 700 to 830 °C, and that of GRMs ranged from 830 to 890 °C. An additional short interference measurement run was conducted using the peak-hopping method on the SEM (IC 1C) to measure the masses of 233 and 231 (i.e., $^{185}ReO_3^-$ and $^{183}WO_3^-$) for each filament measurement. Each run included one block of 10 cycles with integration and idle times of 4 and 3 s, respectively, for a total analysis time of approximately 1.2 min (Table 3: Interf.).

Table 2
The cup configuration for Os isotope static analysis using FCs and CDDs by NTIMS.

Collector	IC5	IC6	L4	L3	L2	L1	C	H1	H2	H3	H4
Type	CDD	CDD	10^{13} Ω	10^{13} Ω	10^{12} Ω	10^{12} Ω	10^{12} Ω	10^{12} Ω	10^{13} Ω	10^{13} Ω	10^{13} Ω
Mass	230	232	234	235	236	237	238	240	241	242	243
Ion beam	$^{198}PtO_2$	$^{184}OsO_3$	$^{186}OsO_3$	$^{187}OsO_3$	$^{188}OsO_3$	$^{189}OsO_3$	$^{190}OsO_3$	$^{192}Os^{16}O_3$	$^{192}Os^{16}O_2^{17}O$	$^{192}Os^{16}O_2^{18}O$	$^{195}PtO_3$

Table 3
Measurement parameters.

		Configuration	Method	Blocks	Cycles	In. (s)	N.I.	Id. (s)	F.T. (°C)
S.S.	Seq.1	FC (10^{12} + 10^{13} Ω Amp.) + CDDs	Static FCs + CDDs	10	20	8	1	12	700–830
	Seq.2	SEM (IC 1C)	Multi-step			4		3	
R.S.	Same as Seq.1								830–890
S.S./R.S.	Interf.	SEM (IC 1C)	Peak hopping	1	10	4	1	3	Same as Sample

S.S.: Solution standard (single-element RMs); R.S.: Rock standard (geological RMs); Seq. 1: Main sequence for Os analysis; Seq. 2: Subsequence for $^{184}OsO_3^-$ analysis using SEM; Interf.: Interference measurement for W and Re; In.: integration time; N.I.: number of integrations; Id.: idle time; F.T.: filament temperature.

2.6. Data processing

Following the measurements, the data were exported and reprocessed offline. In the first step, the cycle-by-cycle correction of isobaric interferences of PtO_2^- and PtO_3^- on OsO_3^- was conducted (the interferences corresponding to each target mass number are listed in Table 4). The ion beams of $^{183}WO_3^-$ and $^{185}ReO_3^-$ were analyzed using pre- and post-run SEM (IC IC) peak-hopping measurement routines. Subsequently, the isobaric interferences of $^{184}WO_3^-$, $^{186}WO_3^-$, and $^{187}ReO_3^-$ were calculated from $^{183}WO_3^-$ and $^{185}ReO_3^-$ and then subtracted from $^{184}OsO_3^-$, $^{186}OsO_3^-$ and $^{187}OsO_3^-$. However, $^{183}WO_3^-$ is itself subject to significant isobaric interference from the heavy oxides of PtO_2^- (Table 4: Mass 231), which can be corrected by measuring the mean interference value of $^{198}PtO_2^-$ using IC5 for each measurement. The calculation of isobaric interference signals of Re, Pt, and W to Os depend on the natural abundance ratios [28], namely, $^{187}Re/^{185}Re = 1.6738$; $^{182}W/^{183}W = 1.8519$; $^{184}W/^{183}W = 2.1412$; $^{186}W/^{183}W = 1.9867$; $^{190}Pt/^{198}Pt = 0.0016$; $^{192}Pt/^{198}Pt = 0.1063$; $^{194}Pt/^{198}Pt = 4.4676$; $^{195}Pt/^{198}Pt = 4.5915$; and $^{196}Pt/^{198}Pt = 3.4273$.

Second, the oxygen isotope composition was calculated. The oxygen isotope composition was determined in-run using measurements of masses of 240, 241, and 242, corresponding to $^{192}Os^{16}O_3^-$, $^{192}Os^{16}O_2^{17}O^-$, and $^{192}Os^{16}O_2^{18}O^-$, respectively (Table 2). To obtain the signal intensities at masses of 240, 241, and 242 corresponding to the net signals of $^{192}Os^{16}O_3^-$, $^{192}Os^{16}O_2^{17}O^-$, and $^{192}Os^{16}O_2^{18}O^-$, respectively, we stripped the mass peaks of masses of 240, 241, and 242 of the various OsO_3 interferences using the O isotopic composition of Nier [37]. The calculation method for $^{17}O/^{16}O$ and $^{18}O/^{16}O$ followed that of Chu et al. (2015) [31].

In the third step, the oxygen isotopic interference was corrected using the mean values of the oxygen isotope composition analyzed in-run.

In the fourth step, the instrumental mass fractionation was corrected using $^{192}Os/^{188}Os = 3.083$ with an exponential law, which was consistent with the most recent $^{192}Os/^{188}Os$ measurements conducted by NTIMS [10,25,26,38]. Mass fractionation corrections of the oxygen isotopes were not applied to the data processing as the mass fractionation of oxygen isotopes can occur during oxygen preparation, activator ($Ba(OH)_2/Ba(NO_3)_2$) preparation, and filament heating, and cannot be quantified. However, the oxygen isotope composition was consistent in one measurement, which was confirmed in our experiments (Section 3.4). Therefore, the oxygen isotope compositions obtained in-run were used for calculations in one measurement, whereas the correction of mass fractionation was conducted on the oxide Os isotopes.

The final step in data processing for each analysis was the rejection of individual integrations outside two standard deviations (SDs) of the mean value for the analysis.

3. Results and discussion

The long-term repeatability of the SRMs was based on the results obtained over a period of 24 months from May 2019 to May 2021 at different intensities by individually adjusting the evaporation filament current. The repeatability of the three GRMs was calculated using three measurements for each sample. The repeatability values (2RSD) are expressed in ‰.

3.1. Analytical results for the Os of SRMs

We present the data obtained from two isotopically distinct Os SRMs that were used to assess the quality of ^{184}Os, ^{186}Os, and ^{187}Os measurements using NTIMS or MC-ICP-MS in previous studies. The ion beam of $^{192}Os^{16}O_3^-$ was measured from 0.04 to 1.0 V for DROsS and from 0.04 to 0.5 V for LOsT in our study. The ion beams of $^{192}Os^{16}O_3^-$ were divided into several data sections to assess their corresponding accuracy and precision values: 0.8–1.0, 0.4–0.5, 0.2–0.3, 0.1–0.16, and 0.04–0.06 V.

3.1.1. The accuracy and precision of $^{184}Os/^{188}Os$

Among the seven Os isotopes, ^{184}Os has the lowest natural abundance (0.02%). Although the signal/noise ratio of the 10^{13} Ω amplifier is theoretically 10 times of that of the 10^{11} Ω amplifier, and the use of the 10^{13} Ω amplifier could significantly improve the measurement precision at low signals, our previous study showed that the precision by SEM is better than that by FCs with 10^{13} Ω amplifiers when the signal is less than 0.4 mV (~20 kcps) [32]. In this study, the ion beam intensity of $^{184}Os^{l6}O_3^-$ was determined between 1100 and 27,000 cps (approximately 21 and 520 μV), implying that the use of SEM to analyze $^{184}Os^{l6}O_3^-$ is the best choice for obtaining optimal precision.

The results show that the $^{184}Os/^{188}Os$ ratios and repeatabilities of the solutions of DROsS and LOsT are almost the same at the 0.04–0.5-V signal of $^{192}Os^{16}O_3^-$, namely, 0.0013010 (28) (2 SD, n = 58, t = 12 months) and 0.0013014 (27) (2 SD, n = 55, t = 12 months), respectively. Our data are consistent with the published data [25,27] in the error range and had better precision, and the ion beam intensity for the

Table 4
The main known or potential polyatomic interferences in the mass spectrum of OsO_3^- ions during NTIMS analysis (O isotope interferences of Os are not included).

Mass	231	232	234	235	238	240	242
Ion beam	$^{183}W^{16}O_3^-$	$^{184}Os^{16}O_3^-$	$^{186}Os^{16}O_3^-$	$^{187}Os^{16}O_3^-$	$^{190}Os^{16}O_3^-$	$^{192}Os^{16}O_3^-$	$^{192}Os^{16}O_2^{18}O^-$
Polyatomic interferences	$^{195}Pt^{18}O_2^-$	$^{184}W^{16}O_3^-$	$^{186}W^{16}O_3^-$	$^{187}Re^{16}O_3^-$	$^{190}Pt^{16}O_3^-$	$^{192}Pt^{16}O_3^-$	$^{194}Pt^{16}O_3^-$
	$^{196}Pt^{17}O^{18}O^-$	$^{196}Pt^{18}O_2^-$	$^{182}W^{16}O^{18}O_2^-$				
	$^{198}Pt^{16}O^{17}O^-$	$^{198}Pt^{17}O_2^-$	$^{182}W^{17}O_2^{18}O^-$				
		$^{198}Pt^{16}O^{18}O^-$	$^{183}W^{17}O_3^-$				
			$^{183}W^{16}O^{17}O^{18}O^-$				
			$^{184}W^{16}O^{17}O_2^-$				
			$^{184}W^{16}O_2^{18}O^-$				
			$^{198}Pt^{18}O_2^-$				
			$^{185}Re^{16}O_2^{17}O^-$				

analysis was only 1/100 to 1/10 of the latter (Table 5). Simultaneously, when the ion beam intensities of $^{192}Os^{16}O_3^-$ are between 0.8 and 1.0 V, the $^{184}Os/^{188}Os$ ratio was 0.0013056 (28) (2 SD, n = 10). Although this value is the same as those measured by FCs with 10^{11} Ω amplifiers on NTIMS [25,27], it is slightly higher than those measured on the 0.04–0.5-V signal of $^{192}Os^{16}O_3$ (Fig. 1a). Additionally, the $^{184}Os/^{188}Os$ ratios of LOsT slightly increased with the ion beam of $^{192}Os^{16}O_3^-$ from the 0.04–0.5-V solution, whereas this trend was not observed for the loadings of DROsS (Fig. 1a and b). As the analyzed signals of $^{184}Os^{l6}O_3^-$ were as low as 17–430 μV, PtO_2^- and WO_3^- ions might have a significant interfering effect on $^{184}Os^{l6}O_3^-$. The ion beam of PtO_2^- and WO_3^- are monitored using an analytical procedure. The results show that the intensity of $^{198}PtO_2^-$ was approximately 1/2 to 1/10 that of $^{184}Os^{l6}O_3^-$ (Fig. 1c). Nevertheless, the intensity of PtO_2^- at the mass peak of 232 is only 1–3‰ for $^{184}Os^{l6}O_3^-$ ions owing to the low abundance of ^{17}O and ^{18}O relative to ^{16}O (Table 4). Moreover, the signals of $^{183}WO_3^-$ are always less than 1‰ of $^{184}Os^{l6}O_3^-$ ions. Accordingly, the interference from PtO_2^- and $^{183}WO_3^-$ was less than 4.3‰ of the total signal at a mass of 232. The intensities of both are the lowest at 0.05 V for $^{192}Os^{l6}O_3^-$ ions, which is less than 1‰ of the total signal at a mass of 232. We did a 600-step mass scan from mass of 216–231 on 1 V signal of $^{192}Os^{16}O_3^-$. The results showed that no interference signals existed at mass of 230 and 231 for $^{198}PtO_2$ and $^{183}WO_3$, respectively. Therefore, the difference in the $^{184}Os/^{188}Os$ ratios of DROsS and LOsT should not be due to overcorrection of PtO_2 and WO_3. It is possible that one or more unknown $^{184}Os^{l6}O_3^-$ (mass of 232) interfering molecules appeared with increasing temperature during the measurement.

The signals of both $^{198}PtO_2^-$ and $^{183}WO_3^-$ were positively but not linearly correlated with that of $^{184}OsO_3^-$ (i.e., temperature) (Fig. 1c and d). This means that both $^{198}PtO_2^-$ and $^{183}WO_3^-$ ion beam might come from the Pt filament. In previous study, Nowell et al. (2008) [26] measured the $^{184}Os/^{188}Os$ ratios at 20–30- and 4–8-V signals of $^{192}Os^{16}O_3^-$using MC-ICP-MS and TIMS, respectively, for the same LOsT solution. The results indicated that the ratios of $^{184}Os/^{188}Os$ by NTIMS were systematically higher than those obtained by MC-ICP-MS. We agree with Luguet [25], who stated that 0.001300 is the best estimate of the true $^{184}Os/^{188}Os$ ratio, and the difference in $^{184}Os/^{188}Os$ between the results of MC-ICP-MS and NTIMS might be ascribed to the isobaric interference of oxide molecules or the error of the deoxidation calculation. The value is likely to be more accurate when the analysis is conducted using MC-ICP-MS in the positive mode. The results from our static measurements using FCs with 10^{13} Ω amplifiers and SEMs imply that the accuracy of the $^{184}Os/^{188}Os$ ratio is more reliable when $^{192}Os^{16}O_3^-$ is measured at ≤0.5 V.

3.1.2. *The accuracy and precision of $^{186}Os/^{188}Os$ and $^{187}Os/^{188}Os$*

LOsT and DROsS were measured at approximately 0.5, 0.25, 0.1, and 0.05 V for the ion beam of $^{192}Os^{l6}O_3^-$. Additionally, a set of $^{192}Os^{l6}O_3^-$ signals ranging from 0.8 to 1.0 V was measured for the DROsS solution. The results are summarized in Table 6. The results indicate that the ratios of $^{186}Os/^{188}Os$ and $^{187}Os/^{188}Os$ are consistent with the published data within the error range, even though the ion beam intensities estimated by our method are only 1/10 to 1/100 of those by conventional methods. The precisions of the $^{187}Os/^{188}Os$ and $^{186}Os/^{188}Os$ ratios from DROsS and LosT were similar at the same ion beam intensities (Table 6 and Fig. 2). The repeatability of $^{186}Os/^{188}Os$ and $^{187}Os/^{188}Os$ ratios could be 0.50–0.60‰ when the ion beam intensities of $^{186}Os^{l6}O_3^-$ and $^{187}Os^{l6}O_3^-$ are as low as 2 mV. The precisions of the $^{187}Os/^{188}Os$ ratio obtained in this work is in agreement with those obtained in our earlier work for calibration solutions of DROsS, Merk-Os and JMC-Os at the same ion beam intensity [32,34].

In a previous study, Luguet (2008) [25] measured a DROsS solution using FCs with a 10^{11} Ω amplifier at a signal of 4–8 V for $^{192}Os^{l6}O_3^-$, obtaining a repeatability values of 0.048 and 0.025‰ for $^{186}Os/^{188}Os$ and $^{187}Os/^{188}Os$, respectively. Liu (2014) [30] measured the DROsS solution using FCs with a 10^{12} Ω amplifier at 0.04–0.95 V for $^{192}Os^{l6}O_3^-$, obtaining repeatability values of 3.12–0.24 and 3.02–0.49‰ for $^{186}Os/^{188}Os$ and $^{187}Os/^{188}Os$, respectively. In this study, when the $^{192}Os^{16}O_3^-$ signal was 0.9–1.0 V, the repeatability values of the $^{186}Os/^{188}Os$ and $^{187}Os/^{188}Os$ ratios of DROsS were 0.066 and 0.065‰, respectively. These values are similar to those measured by Chu et al. (2015) [31] at signals of 6–8 V for $^{192}Os^{16}O_3^-$ using FCs connected with conventional 10^{11} Ω amplifiers and are considerably better than those measured by Liu et al. (2014) [30] with a factor of 3–7 at signals of 0.47–0.95 V for $^{192}Os^{16}O_3$ using FCs connected with 10^{12} Ω amplifiers. When the $^{192}Os^{16}O_3$ signal is approximately 0.5 V, the repeatability values of both DROsS and LOsT for the $^{186}Os/^{188}Os$ and $^{187}Os/^{188}Os$ ratios measured by FCs connected with a 10^{13} Ω amplifier are between 0.072 and 0.14‰, which are as good as those measured by Nowell et al. (2008) [26] at 30 V by MC-ICP-MS and at 4–8 V by NTIMS (both for $^{192}Os^{16}O_3^-$ signals) using FCs connected with 10^{11} Ω amplifiers. The precision obtained by our analysis for $^{186}Os/^{188}Os$ (0.066‰) and $^{187}Os/^{188}Os$ (0.065‰) at 0.9–1.0 V of $^{192}Os^{16}O_3^-$ is slightly larger than those obtained at 4–8 V of $^{192}Os^{16}O_3^-$ by Luguet et al. (0.025–0.048‰) [25] and Chatterjee et al. (0.016–0.024‰) [27] using NTIMS by FC connected with 10^{11} Ω amplifiers. Considering that the analysis data is only 200 for one measurement and the integration time for each cycle is 8 s in this work, and that both the counting statistics and baseline noise are inversely proportional to the integration time and the analysis data, it is theoretically possible to further improve the precision by increasing the integration time and analysis data. In the results of Reisberg et al. (2021) [33], the precision of $^{186}Os/^{188}Os$ is 0.119936 (12) at signals of 0.1–0.18 V for $^{192}Os^{16}O_3^-$, which is as good as our value of 0.119944 (13) at 0.4–0.5 V for $^{192}Os^{16}O_3^-$, whereas we simultaneously obtained a

Table 5
The accuracy and precision of $^{184}Os/^{188}Os$ ratios of LOsT and DROsS.

	$^{192}OsO_3$ (V)	$^{184}OsO_3$ (mV)	$^{184}Os/^{188}Os$	n	Collector configuration	Instrument
LOsT[a]	0.04–0.5	0.02–0.2	0.001301 (3)	55	CDDs + FCs (10^{13} +10^{12} Ω)	NTIMS
LOsT[b]	30	14	0.001302 (10)	11	FCs (10^{11} Ω)	MC-ICPMS
	20	10	0.001303 (24)	12		
	4–8	2.0–3.9	0.001310 (16)	7		NTIMS
DROsS[a]	0.9–1.0	0.4	0.001306 (3)	10	CDDs + FCs (10^{13} +10^{12} Ω)	NTIMS
	0.04–0.5	0.02–0.2	0.001301 (3)	58		
DROsS[c]	4–8	2.0–3.9	0.001305 (5)	8	FCs (10^{11} Ω)	NTIMS
DROsS[d]	7	3.4	0.001305 (2)	8		

[a] This study.
[b] Nowell (2008) [26].
[c] Luguet (2008) [25].
[d] Chatterjee (2015) [27]; the last two digits of uncertainty (2SD) are in parentheses after the $^{184}Os/^{188}Os$ ratio; "FCs (10^{13} +10^{12} Ω)" denotes the FCs connected with $10^{13}/10^{12}$ Ω amplifiers. These expressions are the same as those listed in the following tables.

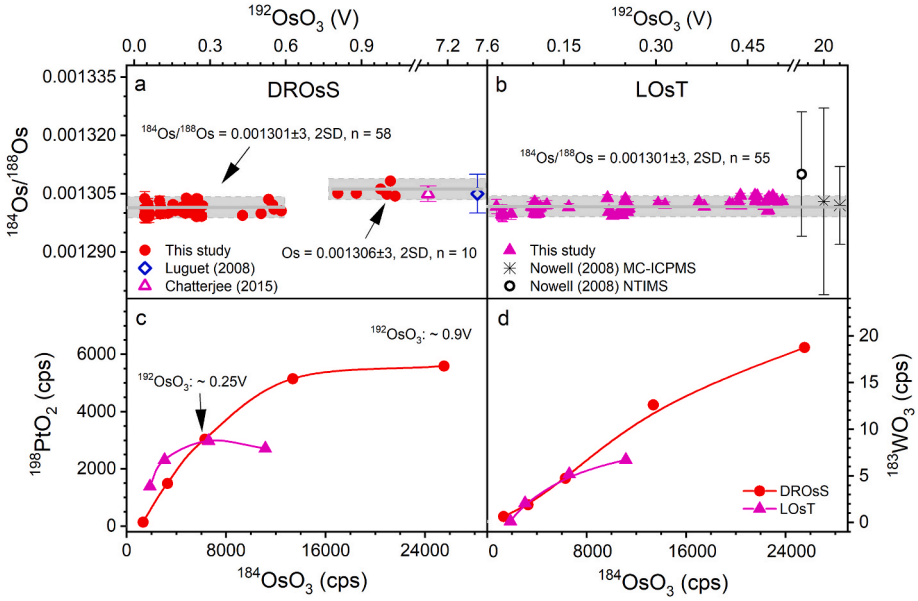

Fig. 1. Accuracy and precision of $^{184}Os/^{188}Os$ and the interference of PtO_2 and WO_3. (a), (b) Correlation between $^{192}Os^{16}O_3^-$ and $^{184}Os^{16}O_3^-$ signals of DROsS and LOsT. The $^{192}Os^{16}O_3^-$ signals is the upper abscissa. The hollow symbols are data from the literature which is same as that in Table 5; (c) Correlation between $^{198}PtO_2^-$ and $^{184}OsO_3^-$ signals. The intensity of $^{198}PtO_2^-$ ions is marked in the left ordinate; (d) Correlation between $^{183}WO_3^-$ and $^{184}OsO_3^-$ signals. The intensity of $^{183}WO_3^-$ ions is marked in the right ordinate.

Table 6
The accuracy and precision of $^{186}Os/^{188}Os$ and $^{187}Os/^{188}Os$ ratios of LOsT and DROsS.

	$^{192}OsO_3^-$ (V)	$^{186}OsO_3^-$ (mV)	$^{187}OsO_3^-$ (mV)	$^{186}Os/^{188}Os$	$^{187}Os/^{188}Os$	n	Collector configuration
LosT[a]	0.4–0.5	18	16	0.119852 (12)	0.106919 (15)	12	CDDs + FCs (10^{13} +10^{12} Ω)
	0.2–0.3	10	9	0.119851 (22)	0.106924 (23)	20	
	0.1–0.2	4	4	0.119848 (47)	0.106924 (34)	16	
	0.04–0.06	2	2	0.119865 (74)	0.106913 (56)	7	
LosT[b]	30			0.119816 (15)	0.106921 (12)	11	FCs (10^{11} Ω)
	20			0.119815 (19)	0.106859 (36)	12	
	4–8			0.119828 (16)	0.106917 (15)	7	
DROsS[a]	0.9–1.0	38	51	0.119946 (8)	0.160928 (10)	10	CDDs + FCs (10^{13} +10^{12} Ω)
	0.4–0.5	18	24	0.119944 (13)	0.160926 (11)	9	
	0.2–0.3	10	14	0.119951 (18)	0.160925 (14)	20	
	0.1–0.2	5	7	0.119953 (34)	0.160928 (25)	23	
	0.04–0.06	2	3	0.119937 (79)	0.160942 (27)	6	
DROsS[c]	4–8			0.119929 (6)	0.160924 (4)	8	FCs (10^{11} Ω)
DROsS[d]	7			0.119930 (3)	0.160922 (3)	8	
DROsS[e]	6–8			0.119933 (6)	0.160920 (12)	15	
DROsS[f]	0.47–0.95			0.119947 (29)	0.160938 (79)	13	FCs (10^{12} + 10^{11} Ω)
	0.04–0.05			0.119860 (374)	0.160890 (486)	14	
	0.005–0.019			0.11994 (157)	0.16104 (131)	18	
DROsS[g]	0.01			0.119949 (197	0.160922 (1187)	1	FCs (10^{13} + 10^{11} Ω)
	0.03–0.09			0.119951 (42)	0.160975 (364)	17	
	0.1–0.18			0.119936 (12)	0.160959 (56)	11	

All data in this table were measured by NTIMS, except for the two ion beams of $^{192}OsO_3^-$ at 30 and 20 V by MC-ICP-MS in the positive ion mode. [a–d] are the same as those in Table 5; [e] Chu (2015a) [31]; [f] Liu (2014) [30]; [g] Reisberg (2021) [33]. The signals of $^{186}OsO_3^-$ and $^{187}OsO_3^-$ are the average values corresponding to the data sections of the $^{192}OsO_3^-$ signal.

similar precision of $^{187}Os/^{188}Os$ of 0.160926 (11) and a high precision of $^{184}Os/^{188}Os$ of 0.001301(3).

3.2. Analytical results for the GRMs

Three GRMs samples, namely, WPR-1, BIR-1a, and BHVO-2, were analyzed in our study. The $^{187}Os/^{188}Os$ ratios of these three rock samples analyzed by FCs or SEM have been widely reported as they represent typical mantle lithology and cover the Os mass fraction of most mantle rocks. However, the $^{184}Os/^{188}Os$ and $^{186}Os/^{188}Os$ ratios of the GRMs have rarely been reported. Among three GRM samples, the amount of Os analyzed in altered peridotite WPR-1 was the largest, at approximately 12 ng, and was measured at signals of 0.23–0.36 V for $^{192}OsO_3^-$; the maximum Os analyzed in basalt BIR-1a was 306 pg, measured at signals of 12–25 mV for $^{192}OsO_3^-$; and the amount of Os analyzed in basalt BHVO-2 was the lowest, at approximately 66 pg, and was measured at signals of 5–7 mV for $^{192}OsO_3^-$. All $^{184}Os/^{188}Os$ ratios of the three GRMs were in accordance with those of the SRMs in the error range (Tables 5 and 7). The $^{184}Os/^{188}Os$ ratio of WPR-1, BIR-1a, and BHVO-2 were 0.001300 (3), 0.001275 (46), and 0.001324 (116) (n = 3), respectively. The poor precision of the $^{184}Os/^{188}Os$ ratio of BIR-1a and BHVO-2 was ascribed to the extremely low $^{184}OsO_3^-$ signals (<700 cps/13 μV).

The $^{186}Os/^{188}Os$ and $^{187}Os/^{188}Os$ ratios of WPR-1 coincide with those of Chu (2015a) [31], which were measured by FCs with 10^{11} Ω

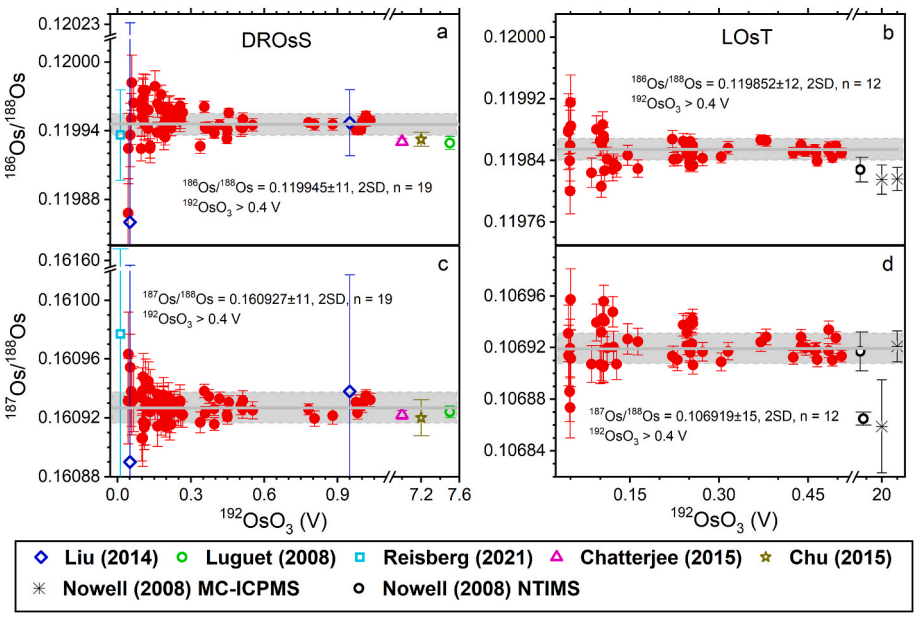

Fig. 2. Accuracy and precision of $^{186}Os/^{188}Os$ and $^{187}Os/^{188}Os$ of DROsS and LOsT.

Table 7
The ratios of $^{184}Os/^{188}Os$, $^{186}Os/^{188}Os$, and $^{187}Os/^{188}Os$ for three GRMs.

	$^{192}OsO_3$ (V)	$^{184}OsO_3$ (Cps)	$^{186}OsO_3$ (mV)	$^{187}OsO_3$ (mV)	$^{184}Os/^{188}Os$	$^{186}Os/^{188}Os$	$^{187}Os/^{188}Os$	n	Collector configuration
WPR-1[a]	0.23–0.36	8200	12	15	0.001300(3)	0.119869(7)	0.144558(7)	3	CDDs + FCs (10^{13} +10^{12} Ω)
WPR-1[e]	3.8				–	0.119845(10)	0.144558(81)	4	FCs (10^{11} Ω)
WPR-1[h]	0.23				–	–	0.144267(22)	3	FCs (10^{13}+10^{12} Ω)
	0.24				–	–	0.144337(48)	3	
BIR-1a[a]	0.01–0.03	550	0.7	0.8	0.001275(46)	0.120428(42)	0.133107(499)	3	CDDs + FCs (10^{13} +10^{12} Ω)
BIR-1a[h]	0.03				–	–	0.133184(336)	3	FCs (10^{13}+10^{12} Ω)
BIR-1a[i]	0.05				–	–	0.13347 (16)	4	FCs (10^{11} Ω)FCs (10^{11} Ω)
BIR-1a[j]					–	–	0.13372 (80)	8	
BHVO-2[a]	0.005–0.007	280	0.3	0.3	0.00132(12)	0.12131(186)	0.14677(139)	3	CDDs + FCs (10^{13} +10^{12} Ω)
BHVO-2[h]	0.008				–	–	0.135100(762)	3	FCs (10^{13}+10^{12} Ω)
	0.007				–	–	0.151570(415)	3	
BHVO-2[i]					–	–	0.14653 (786)	6	FCs (10^{11} Ω)

[a] This study.
[e] Chu (2015a) [31].
[h] Wang (2019) [34].
[i] Chu (2015b) [39].
[j] Ishikawa (2014) [40]. The signals of $^{184}OsO_3$, $^{186}OsO_3$, and $^{187}OsO_3$ are the average values corresponding to the data sections of the $^{192}OsO_3$ signal.

amplifiers at intensities of 3.8 V for $^{192}OsO_3^-$ (Table 5). Although the $^{192}OsO_3^-$ intensities are less than 1/10 of those of Chu (2015a) [31] and the sample size is 1/2 of that in their study, our data show better precision. The $^{187}Os/^{188}Os$ ratios of BIR-1a and BHVO-2 are also in agreement with published data measured using FCs with 10^{11} Ω amplifiers [39,40]. Each of the three GRM samples had less than half the sample size used in the literature. Additionally, the $^{187}Os/^{188}Os$ ratios of BIR-1a and BHVO-2 are consistent with our previous results measured using FCs with 10^{13} Ω amplifiers [34]. Overall, the new method is suitable for the Os isotope analysis of rock samples.

[a] This study; [e] Chu (2015a) [31]; [h] Wang (2019) [34]; [i] Chu (2015b) [39]; [j] Ishikawa (2014) [40]. The signals of $^{184}OsO_3$, $^{186}OsO_3$, and $^{187}OsO_3$ are the average values corresponding to the data sections of the $^{192}OsO_3$ signal.

3.3. Factors influencing the precision and accuracy of ^{184}Os

To date, no studies have determined ^{184}Os in samples with low amounts of Os (<20 ng) because of its extremely low abundance (~0.02% in nature). Only a few $^{184}Os/^{188}Os$ datasets exist for samples with large amounts of Os (>40 ng) [25,27]. The main difficulty is obtaining high accuracy and precision of $^{184}Os/^{188}Os$ ratios at a low ion beam intensity of $^{184}OsO_3^-$ (e.g., <0.5 mV). In this study, an ion beam of $^{184}OsO_3^-$ was collected by a CDD (IC6) to minimize the impact of noise interference. Theoretically, this ensures high-precision data for a smaller sample size. The extremely low abundance of ^{184}Os makes it sensitive to interfering ions and measurement parameters. Thus, it is necessary to discuss the factors that could influence the accuracy and precision of ^{184}Os determination.

3.3.1. Zoom Optics parameters and the operating voltage of IC6

Appropriate cup configuration and optical parameters are necessary

to ensure analytical accuracy and precision. IC6 is mounted and fixed on the detector of an L4 cup. Dispersion and focus of 33.0 and −8.0 V, respectively, were used to optimize the peak overlap. After adjusting the zoom optics, the peak overlap in all cup and IC configurations realized ion collection at the same spot within the cup. Although the peak shape of IC6 is slightly narrower, the data acquisition interval is consistent with the flat-top peaks of other oxide molecules and does not affect the accuracy of $^{184}OsO_3^-$ determination (Fig. 3).

Notably, the detection results show that the peak shape of IC6 is more sensitive to the operating voltage than those of IC5 and SEM (IC 1C)). IC5 and SEM (IC 1C) always exhibited a flat peak shape when the operating voltage was adjusted to yield values from 90 to 100%. Nevertheless, the ion beam peak shape of IC6 was flat only when the yield was greater than 98% (Fig. 4a). Our results show that the ratios of $^{184}Os/^{188}Os$ are stable and the same as those in the literature only when the yield of IC6 is greater than 98%; otherwise, the ratios are distinctly lower (Fig. 4b).

3.3.2. Measurement model (static/peak-hopping)

The internal precisions of $^{184}Os/^{188}Os$ are similar and less than 1×10^{-6} (2 SE, n = 200) in one measurement, regardless of whether $^{184}OsO_3^-$ was analyzed by IC6 or SEM (IC 1C)) (Fig. 5a). The long-term repeatability of the $^{184}Os/^{188}Os$ ratio is 0.001301 (2) (2 SD, n = 38) when the ion beam intensity of $^{184}OsO_3^-$ ranged from approximately 1100 cps (21 μV) to 13,000 cps (250 μV) by IC6 (Fig. 5b). Under the same conditions, the long-term repeatability of the $^{184}Os/^{188}Os$ ratio was 0.001312 (13) (2 SD, n = 47), as determined using SEM SEMs (IC 1C) (Fig. 5b). The results show the long-term repeatability of $^{184}Os/^{188}Os$, of which the $^{184}OsO_3^-$ ion beam analyzed by IC6 is approximately six times better than that analyzed by SEM (IC 1C) (Fig. 5b). The improved precision of $^{184}OsO_3^-$ by IC6 can be ascribed to the static measurement of IC6 and other FCs relative to the jump-hopping of SEM (IC 1C).

3.4. Heavy oxide corrections

The accuracy and precision of Os isotope ratios could be affected by variations in oxygen isotope ratios as Os isotopes are measured as OsO_3^- ions by NTIMS. In previous studies, O isotopes were either determined using multistep dynamic analysis or static measurement with the simultaneous determination of major Os isotopes and oxygen isotope compositions; however, several Os isotopes had to be omitted. This is due to the difficulty in aligning the FCs to collect the main $Os^{16}O_3^-$ isotopes and two heavy oxygen atoms from masses of 241 and 242, which essentially comprise $^{192}Os^{16}O_2^{17}O^-$ and $^{192}Os^{16}O_2^{18}O^-$ in one static collection. In this study, a new static method was used to simultaneously measure all Os isotopes and O isotopes. The results showed that the mass fractionation of oxygen isotopes was very small in one measurement but could be large in different measurements, which might be attributed to the different volumes of added O_2 and the filament temperatures in different measurements. The internal precision of the $^{18}O/^{16}Os$ ratio is commonly approximately 0.20‰ (2RSE, n = 200) during a single run, and the long-term repeatability of the $^{18}O/^{16}Os$ ratio is approximately 20‰ (2RSD, n = 140) during two years (Fig. 6a and b). The O isotope compositions of DROsS and LOsT approximately showed the same range of variation; however, the data were not correlated well (Fig. 6b). We measured a filament-loaded DROsS with 20 ng of Os at the same filament current (1608 mA), same ion beam intensity of $^{192}OsO_3^-$ (0.25 V), and same volume of added oxygen (the high vacuum (HV) source pressure was 2.47×10^{-7} mbar). The $^{17}O/^{16}O$ and $^{18}O/^{16}O$ ratios from the three measurements defined a mass fractionation line with a slope of 0.157 and $R^2 = 0.999$. The same heating current (1608 mA) was maintained in the fourth measurement of this filament as in the previous three analyses, and the volume of added oxygen was halved (HV was at 2.05×10^{-7} mbar, based on a HV of 1.60×10^{-7} without added O_2). As a result of the reduction in added oxygen, the $^{192}OsO_3^-$ ion intensity decreased to 0.15 V. The $^{17}O/^{16}O$ and $^{18}O/^{16}O$ ratios obtained in the fourth measurement significantly deviated from the mass fractionation line defined in the previous three analyses (Fig. 6c). Although many reasons exist for the variation in O isotope mass fractionation, our results show that different volumes of added oxygen significantly affect the variation in the O isotope mass fractionation during the determination of Os isotopes.

Considering that the ratios of $^{17}O/^{16}O$ and $^{18}O/^{16}O$ can vary greatly between different measurements, high-precision data should be obtained using in-run measurements rather than fixed values of O isotopic composition. Using our new method, it is simple to determine the in-run oxygen composition.

4. Conclusions

We present a novel static method for the high-precision measurement of $^{184}Os/^{188}Os$, $^{186}Os/^{188}Os$, and $^{187}Os/^{188}Os$ ratios using a cup configuration combination of CDDs and FCs with 10^{13} Ω and 10^{12} Ω amplifiers. This cup configuration enabled the simultaneous collection of all Os isotopes, monitoring of the isobaric oxide interference of PtO_2 and PtO_3, and measurement of the oxygen isotopic composition in the run.

By choosing the SEM (CDD) with the highest signal/noise ratio to collect the $^{184}OsO_3^-$ ion beam, our new method can analyze the $^{184}OsO_3^-$ ions with signals as low as 1100 to 27,000 cps (~21–520 μV). An $^{184}Os/^{188}Os$ precision of 2–3‰ was obtained, which was consistent with or better than that analyzed by FCs with a conventional 10^{11} Ω amplifier for $^{184}OsO_3^-$ signals greater than 2 mV. Extrapolating from the measurable $^{184}OsO_3^-$ signal, our newly proposed method only used 1/5 to 1/100 of the sample size of the conventional method to obtain the $^{184}Os/^{188}Os$ ratio with the same precision.

All Os isotopes, except ^{184}Os, were analyzed using a combination of FCs with 10^{13} Ω and 10^{12} Ω amplifiers. The results suggest that the

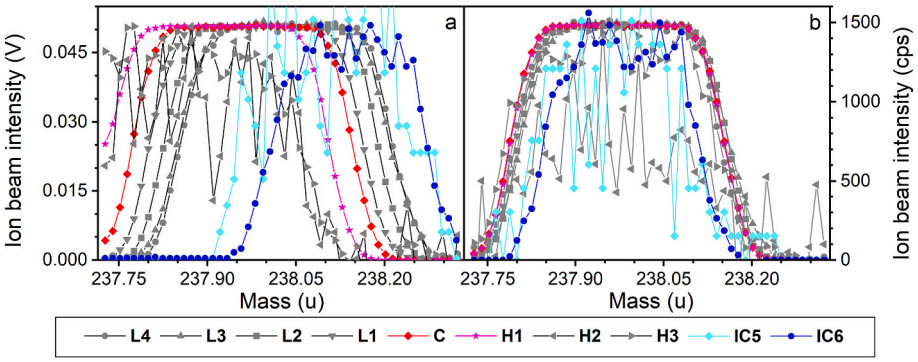

Fig. 3. Zoom parameters vs. peak overlap. (a) Peak overlap using no zoom optics. (b) Peak overlap using zoom optics. IC5 and IC6 collected $^{198}PtO_2$ and $^{184}OsO_3$, respectively, with ion beam intensities of cps indicated by the right ordinate.

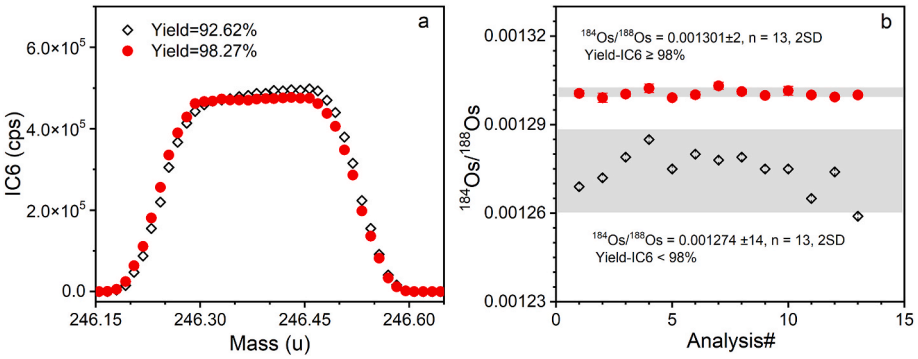

Fig. 4. Influence of operating voltage on yield and peak shape of IC6. (a) The peak shape of ion beam $^{184}OsO_3^-$ by IC6 can be kept flat only at yields >98%. (b) The ratios of $^{184}Os/^{188}Os$ measured by IC6 with yield IC6 ≥ 98% and <98%.

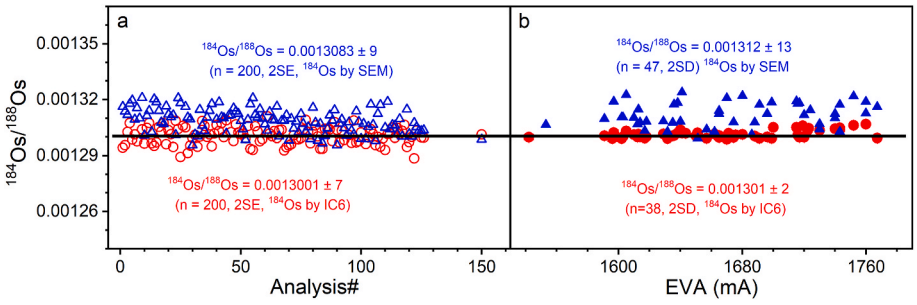

Fig. 5. The accuracy and precision of $^{184}Os/^{188}Os$ ratios. (a) The internal precision of $^{184}Os/^{188}Os$ ratios in which the $^{184}OsO_3^-$ ion beam was analyzed by IC6 (hollow red circles) and SEM (IC 1C)) (hollow blue triangles) depending on one measurement. (b) The long-term repeatability of $^{184}Os/^{188}Os$ ratios in which the $^{184}OsO_3^-$ ion beam was analyzed by IC6 (solid red circles) and SEM (IC 1C)) (solid blue triangles) over approximately 2 years. The black lines in (a) and (b) are the recommended values of $^{184}Os/^{188}Os$ by Luguet [25]. (For interpretation of the references to colour in this figure legend, the reader is referred to the Web version of this article.)

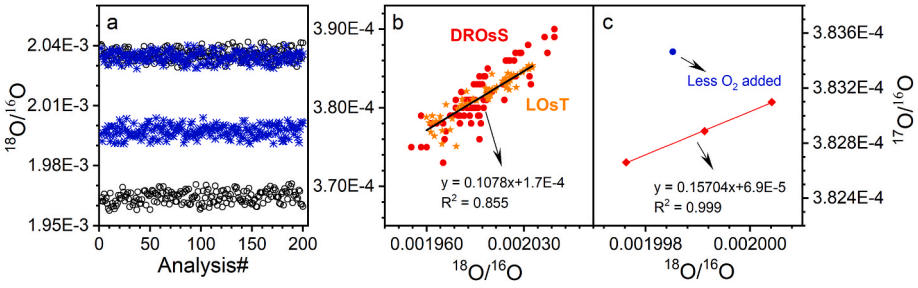

Fig. 6. The variation in oxygen isotopic ratios in each analysis and a batch analysis. (a) The variation of the $^{18}O/^{16}Os$ ratio between one measurement and different measurements; (b) Mass fractionation of O isotopes measurement in run with DROsS and LOST; (c) adjusting the volume oxygen added could cause significant variation of O mass fractionation.

precision of the $^{186}Os/^{188}Os$ and $^{187}Os/^{188}Os$ ratios is 0.066‰ when $^{186}OsO_3^-$ and $^{187}OsO_3^-$ signals are at 30–50 mV. This is consistent with the precision of the $^{186}Os/^{188}Os$ and $^{187}Os/^{188}Os$ ratios measured by FCs with conventional 10^{11} Ω amplifiers when $^{186}OsO_3^-$ and $^{187}OsO_3^-$ signals were greater than 150 mV.

The Os isotope measurements of the three GRM samples show that the new method can be applied to real geological samples with sample sizes of <1 g and Os mass fractions ranging from 13 ng g^{-1} to 76 pg g^{-1}.

Additionally, our results show that oxygen isotopic compositions vary between different filaments and different analyses but are stable in one measurement. This variation can be significant because of the changes in the volume of added oxygen during the measurement. Therefore, the isobaric oxide interference should be corrected based on the oxygen isotopes in each measurement. In this study, we provide a new method for simultaneously obtaining high-precision $^{184}Os/^{188}Os$, $^{186}Os/^{188}Os$, and $^{187}Os/^{188}Os$ ratios when the $^{184}OsO_3^-$ signal is larger than 21 μV and the signals of $^{186}OsO_3^-$ or $^{187}OsO_3^-$ are less than 50 mV.

CRediT authorship contribution statement

Guiqin Wang: Conceptualization, Methodology, Writing – review & editing, Data curation, Funding acquisition. **Yuling Zeng:** Chemical experiments, TIMS measurement. **Liang Qi:** Chemical experiment, Supervision. **Wengui Liu:** TIMS technical, Supervision, Methodology, solved perfectly the technical difficulties of the TIMS method. **Jifeng Xu:** Supervision, Resources.

Declaration of competing interest

The authors declare that they have no known competing financial interests or personal relationships that could have appeared to influence the work reported in this paper.

Data availability

Data will be made available on request.

Acknowledgment

The authors had the great honour of applying for and receiving approval to carry out Os isotope studies on the chang'e-5 lunar samples allocated by the China National Space Administration, and for this purpose we have developed this method for the high-precision measurement of Os isotopes in this sample, as well as in other similar low-content/small-size samples. The authors are grateful to Dr. Meisel, T. C. for providing the LOsT Os solution standards; thanks Dr. Li Jie for his help with chemical experiment. This work was financially supported by the National Key Research and Development Project of China (No. 2020YFA0714804); Strategic Priority Research Program of Chinese Academy of Sciences (No. XDB 41000000); the National Natural Science Foundation of China (No. 42073061); and Pre-research project on Civil Aerospace Technologies by CNSA (No. D020203). This is contribution No. IS-3385 from GIGCAS.

Appendix A. Supplementary data

Supplementary data to this article can be found online at https://doi.org/10.1016/j.aca.2023.341721.

References

[1] S.B. Shirey, R.J. Walker, Annu. Rev. Earth Planet Sci. 26 (1998) 423–500.
[2] J.H. Chen, D.A. Papanastassiou, G.J. Wasserburg, Lunar Planet. Inst. Sci. Conf. Abstr. (2001) 1480.
[3] D. Hnatyshin, R.A. Creaser, J.J. Wilkinson, S.A. Gleeson, Geology 43 (2015) 143–146.
[4] Z. Chu, J. Xu, Adv. Earth Sci. 36 (2021) 245–264.
[5] V.M. Cumming, D. Selby, P.G. Lillis, M.D. Lewan, Geochem. Cosmochim. Acta 138 (2014) 32–56.
[6] J. Pasava, A. Vymazalova, J. Mao, A. Du, W. Qu, W. Korzekwa, 9th Biennial Meeting of the Society for Geology Applied to Mineral Deposits, Dublin, Ireland, 2007, pp. 221–224.
[7] R.J. Walker, J.W. Morgan, M.F. Horan, G.K. Czamanske, E.J. Krogstad, V. A. Fedorenko, V.E. Kunilov, Geochem. Cosmochim. Acta 58 (1994) 4179–4197.
[8] J.W. Morgan, R.J. Walker, M.F. Horan, E.S. Beary, A.J. Naldrett, Geochem. Cosmochim. Acta 66 (2002) 273–290.
[9] D.L. Cook, R.J. Walker, M.F. Horan, J.T. Wasson, J.W. Morgan, Geochem. Cosmochim. Acta 68 (2004) 1413–1431.
[10] A.D. Brandon, R.J. Walker, I.S. Puchtel, Geochem. Cosmochim. Acta 70 (2006) 2093–2103.
[11] R.J. Walker, Geochem. Perspect. 5 (2016) 1–145.
[12] A.C. Hunt, M. Ek, M. Schonbachler, Geochem. Cosmochim. Acta 216 (2017) 82–95.
[13] J.M.D. Day, B. O'Driscoll, Earth Planet Sci. Lett. 519 (2019) 101–108.
[14] R.F. Sperlein, R.L. Wolke, J. Inorg. Nucl. Chem. 38 (1976) 27–29.
[15] E.L. Medeiros, M.M.N. Rodrigues, S.B. Duarte, O.A.P. Tavares, J. Phys. G Nucl. Part. Phys. 32 (2006) B23–B30.
[16] G. Gangopadhyay, J. Phys. G Nucl. Part. Phys. 36 (2009).
[17] S.T.M. Peters, C. Muenker, H. Becker, T. Schulz, Earth Planet Sci. Lett. 391 (2014) 69–76.
[18] A.G.W. Cameron, Publ. Astron. Soc. Pac. 69 (1957) 201–226.
[19] M. Arnould, S. Goriely, Phys. Rep. 384 (2003) 1–84.
[20] Z. Yang, G. Wang, Y. Xu, Y. Zeng, Z. Zhang, Minerals 12 (2022) 759.
[21] J.M.D. Day, M. Paquet, A.J. Timothy Jull, Meteorit. Planet. Sci. 56 (2021) 683–699.
[22] T. Schulz, P.P. Povinec, L. Ferrière, A.J.T. Jull, A. Kováčik, I. Sýkora, J. Tusch, C. Münker, D. Topa, C. Koeberl, Meteorit. Planet. Sci. 55 (2020) 294–311.
[23] P. Gleissner, H. Becker, Geochem. Cosmochim. Acta 200 (2017) 1–24.
[24] K.T. Tait, J.M.D. Day, Earth Planet Sci. Lett. 494 (2018) 99–108.
[25] A. Luguet, G.M. Nowell, D.G. Pearson, Chem. Geol. 248 (2008) 342–362.
[26] G.M. Nowell, A. Luguet, D.G. Pearson, M.S.A. Horstwood, Chem. Geol. 248 (2008) 363–393.
[27] R. Chatterjee, J.C. Lassiter, Chem. Geol. 396 (2015) 112–123.
[28] J. Meija, T.B. Coplen, M. Berglund, W.A. Brand, P.D. Bièvre, M. Gröning, N. E. Holden, J. Irrgeher, R.D. Loss, T. Walczyk, T. Prohaska, Pure Appl. Chem. 88 (2016) 293–306.
[29] J.I. Kimura, T. Nozaki, R. Senda, K. Suzuki, J. Anal. At. Spectrom. 29 (2014) 1483–1490.
[30] J. Liu, D.G. Pearson, Chem. Geol. 363 (2014) 301–311.
[31] Z.-Y. Chu, C.-F. Li, Z. Chen, J.-J. Xu, Y.-K. Di, J.-H. Guo, Anal. Chem. 87 (2015) 8765–8771.
[32] G. Wang, T. Sun, J. Xu, Rapid Commun. Mass Spectrom. 31 (2017) 1616–1622.
[33] L. Reisberg, C. Zimmermann, Geostand. Geoanal. Res. 45 (2021) 287–311.
[34] G. Wang, H. Vollstaedt, J. Xu, W. Liu, Geostand. Geoanal. Res. 43 (2019) 419–433.
[35] J. Li, X.-Y. Jiang, J.-F. Xu, L.-F. Zhong, X.-C. Wang, G.-Q. Wang, P.-P. Zhao, Geostand. Geoanal. Res. 38 (2014) 37–50.
[36] G. Wang, Y. Zeng, J. Xu, W. Liu, J. Mass Spectrom. 53 (2018) 455–464.
[37] A.O. Nier, Phys. Rev. 77 (1950) 789–793.
[38] R.J. Walker, A.D. Brandon, J.M. Bird, P.M. Piccoli, W.F. McDonough, R.D. Ash, Earth Planet Sci. Lett. 230 (2005) 211–226.
[39] Z. Chu, Y. Yan, Z. Chen, J. Guo, Y. Yang, C. Li, Y. Zhang, Geostand. Geoanal. Res. 39 (2015) 151–169.
[40] A. Ishikawa, R. Senda, K. Suzuki, C.W. Dale, T. Meisel, Chem. Geol. 384 (2014) 27–46.